Theoretical investigation of RbCs via two-component spin-orbit pseudopotentials: Spectroscopic constants and permanent dipole moment functions

Ivan S. Lim, Won Chai Lee, and Yoon Sup Lee[a)]
Quantum and Computational Chemistry Lab, Department of Chemistry, Korea Advanced Institute of Science and Technology, 373-1 Guseong-dong, Yuseong-gu, Daejoen 305-701, Korea

Gwang-Hi Jeung
Laboratoire de Chimie Théorique (CNRS UMR6517), Case 521, Campus de St-Jérôme, Université de Provence, 13397 Marseille Cedex 20, France

(Received 22 March 2006; accepted 19 April 2006; published online 16 June 2006)

Potential energy curves for the 28 lowest $\Lambda\Sigma$ states and 49 Ω states of RbCs are obtained from large-scale multireference configuration interaction calculations using both spin-averaged and two-component spin-orbit energy-consistent effective core potentials. Spectroscopic properties of all states are compared across available data in literature to date. Variations of the permanent dipole moments on the internuclear separation (R) for the $^1\Sigma^+$, $^3\Sigma^+$, $^1\Pi$, and $^3\Pi$ states are evaluated over a wide range of R. The most important effects of the spin-orbit interaction on the dipole moment distribution are discussed. © *2006 American Institute of Physics*. [DOI: 10.1063/1.2204607]

I. INTRODUCTION

Over the years alkali metals and their homo-/heteronuclear dimers have received a considerable amount of interest in many fields of chemistry and physics. One of the most prominent developments in recent years includes the production of ultracold molecules.[1–3] This opens new perspectives in areas such as quantum computing[4] as well as providing for new sensitive tests of fundamental theories.[5] RbCs has been recognized as a particularly attractive candidate in these areas attributed to the efficiency with which the constituent atoms can be laser cooled with diode lasers.[6] In the last couple of years, metastable RbCs in electronically excited states have been produced via photoassociation, making it potentially possible to produce large samples of ultracold RbCs molecules.[7]

The theoretical investigation of RbCs has equally been active. There exist a few papers dealing with the potential energy curves for a large number of states.[8,9] Earlier studies have been criticized for the neglect of spin-orbit effects, which posed a particular difficulty in the spectral analysis of RbCs. This has been rectified a few years ago in *ab initio* calculations employing semiempirical pseudopotentials including spin-orbit effects.[10] This study gave the potential energy curves of a vast number of Ω states for the first time and remains to be the only set of such data available to date. There is a growing interest in the radial variation of the permanent and transition dipole moments,[11,12] as such information is valuable for the creation of ultracold samples of RbCs. Although there is a very recent report of a four-component all-electron calculation of the $X\,^1\Sigma^+$ and $a\,^3\Sigma^+$ states of RbCs,[13] which naturally includes spin-orbit effects, dipole moment studies employing pseudopotential approximations have generally neglected spin-orbit effects. On the experimental side, the complex nature of the spin-orbit interaction has been discussed for the laser-induced fluorescence of the coupled $^1\Sigma^+$ and $^3\Pi$ states. The spin-orbit interaction between these states has been utilized to study the triplet states through the perturbation-facilitated optical-optical double-resonance technique.[14] Despite the advances made both on the experimental and theoretical fronts, there is still a strong demand by the experimentalists for an extensive range of information regarding RbCs, including potential energy curves (PECs) and dipole and transition dipole moments functions dependent on the internuclear separation, which is scarcely available in literature. We aim to meet these demands by providing PECs and dipole moment functions of RbCs, giving special emphasis on the spin-orbit interaction.

In this study, we make the first application of nonempirical two-component pseudopotentials developed recently to evaluate the potential energy curves for a large number of electronically excited states of RbCs. This is carried out for the $\Lambda\Sigma$ states, including scalar relativistic effects, and for Ω states resulting from spin-orbit coupling between the $\Lambda\Sigma$ states. Selected spectroscopic constants are determined and compared with the available data. The variation of permanent dipole moments as a function of the internuclear distance, including spin-orbit effects, is also presented.

II. METHOD

For the evaluation of potential energy curves of the $\Lambda\Sigma$ states of RbCs, we used two sets of spin-orbit averaged energy-consistent pseudopotentials (ARPPs) for comparison, namely, that of Leininger *et al.*[15] (PP1) and, more recently, of Lim *et al.* (PP2).[16] For the calculation of Ω states resulting from the $\Omega\Omega$ coupling, two-component spin-orbit pseudopotentials (SOPPs) of Lim *et al.* were used. Details of the fit-

[a)]Electronic mail: yoonsuplee@kaist.ac.kr

TABLE I. Transition energies of Rb and Cs atoms calculated with the ECPs used in this study. Experimental values are taken from Ref. 19. All values are in cm^{-1}.

ARPP		PP1	PP2	Ref. 9	Expt.
Rb	$5s$	0	0	0	0
	$5p$	12681	12698	12737	12737
	$4d$	19366	19506	19355	19355
	$6s$	20134	20057	20101	20134
Cs	$6s$	0	0	0	0
	$6p$	11520	11485	11547	11548
	$5d$	14594	15222	14539	14539
	$7s$	18546	18473	18537	18536
SOPP			PP2	Ref. 10	Expt.
Rb	$5s$	⋯	0	0	0
	$5p_{1/2}$	⋯	12596	12578	12579
	$5p_{3/2}$	⋯	12798	12816	12817
	$4d_{5/2}$	⋯	19531	19355	19355
	$4d_{3/2}$	⋯	19534	19355	19355
	$6s$	⋯	20095	20101	20134
Cs	$6s$	⋯	0	0	0
	$6p_{1/2}$	⋯	11213	11173	11178
	$6p_{3/2}$	⋯	11692	11728	11732
	$5d_{5/2}$	⋯	15224	14481	14499
	$5d_{3/2}$	⋯	15287	14579	14597
	$7s$	⋯	18514	18537	18536

ting procedure are available in the references given above and therefore will be omitted here. Instead, we give a brief description. Both sets are energy-consistent pseudopotentials consisting of nine valence electrons (9-ve). The valence basis sets are also as given in the above references, but the one accompanying the Leininger pseudopotentials was modified slightly as follows: For Rb, the most diffuse *s*- and *p*-type functions were substituted by four diffuse functions for each set (0.1357, 0.0254, 0.005 93, and 0.002 59 for the *s* subset and 0.0285, 0.0110, 0.0032, and 0.0018 for the *p* subset). The contraction was removed, and the resulting set was further augmented by seven *d*-type (0.7513, 0.3312, 0.0963, 0.0324, 0.0144, 0.0071, and 0.003 92) functions and one *f*-type (0.8075) function. For Cs, the *s* subset was extended by an additional diffuse function (0.0039), whereas the *p* subset was entirely replaced by eight functions (4.1953, 1.9707, 0.5830, 0.3423, 0.1503, 0.0304, 0.0122, and 0.004). *d*- and *f*-type functions were also included (0.2960, 0.1043, 0.038 95, 0.016 52, 0.007 37, and 0.0030 for *d* and 0.300 and 0.100 for the *f* subset). For the construction of the potential energy curves, large scale multireference configuration interaction (MRCI) procedures were used for the two valence electrons of RbCs, keeping the rest frozen, i.e., in a full valence CI scheme. Therefore, we employed one-electron (1-e) core-polarization potentials (CPPs) to account for core-valence correlation effects, which were adopted from Ref. 17. Spectroscopic constants were derived from the potential energy curves. To the best of our knowledge, this is the first application of the nonempirical pseudopotentials in a study of potential energy curves of RbCs, including spin-orbit effects. All calculations were carried out with the MOLPRO program package.[18]

Before leaving this section, we present the calculated transition energies for the Rb and Cs in Table I as obtained from a full valence CI calculation using the 9-ve ECP and 1-e CPP, as in the molecular calculations with and without spin-orbit coupling. These values are compared with the experimental values.[19] For the transition energies without spin-orbit coupling, there is a fairly good agreement between ARPP(PP1) and experimental values, whereas the ARPP(PP2) shows a larger deviation from the experiments. For the ARPP(PP2) the most troublesome states are the Rb ($4d$) and Cs ($5d$) states, which, in the case of the latter, deviates from the experimental asymptote by up to 700 cm^{-1}. For other asymptotes, the calculated values are comparable to the experiment, and the accuracy limit is practically reached within the pseudopotential error. The results including spin-orbit effects display similar deviations from the experimental values, with the *d* states showing the largest error. Adjustment of the cutoff parameter for the 1-e CPP gave some improvement for the *d* state, but only at the expense of others. The spin-orbit splitting is, however, well approximated by the PP2. To further improve the accuracy, the angular momentum dependent CPP may be employed.[9,10] This is clearly shown in the work by Allouche *et al.* and also in Table I of this work, confirming a far superior agreement between the experiment and the theoretical values adopting *l*-dependent CPP. All-electron results of Edvardsson *et al.*[20] for the Rb transition energies obtained at the complete active space self-consistent field (CASSCF) level compare more favorably than our results. Although it is possible to correct the molecular energies based on the error estimated for the atomic asymptotes, different atomic configurations intermix in the molecular states in general, and therefore no asymptotic energy compensations were made in our calculated state-to-state transition energies (T_e) for the RbCs states.

III. RESULTS AND DISCUSSION

We first present the spectroscopic constants for the ground state of RbCs obtained in a coupled-cluster with singles, doubles, and pertubative triples [CCSD(T)] calculation in which all 18 electrons outside the core as defined by the 9-ve ECPs were correlated explicitly. Therefore, the CPP in this case accounts for the core-valence correlation on the $(n\text{-}2)$ core of the metal. Spectroscopic constants are obtained as 4.406 Å, 50.34 cm^{-1}, 1.657×10^{-2} cm^{-1}, and 3630 cm^{-1} for the respective equilibrium bond distance, vibrational frequency, rotational constant, and dissociation energy. The equilibrium constants are in best agreement with the experimental data in comparison with other theoretical values reported, while the dissociation energy is somewhat underestimated (see Table II and Ref. 21). It shows that the best result can be expected from an explicit correlation treatment of the 18 electrons when it is technically feasible. The relative disagreement for the CCSD(T) bond energy is an inherent feature of the coupled-cluster method which cannot describe the bond breaking properly in SD and SD(T) levels of approximation.

The calculated PECs for the $^1\Sigma^+$, $^3\Sigma^+$, $^1\Pi$, $^3\Pi$, $^1\Delta$, and $^3\Delta$ states of RbCs resemble closely the previously published ones and therefore are only made available online (see Ref. 22). Selected spectroscopic constants derived from these PECs via the Dunham-type analysis around the minimum are collected in Table II. Important regions of the avoided crossing between the states are well reproduced by the present study. In particular, we note avoided crossings among $^3\Sigma^+$ states, namely, those between (2) and (3), between (5) and (6), and between (6) and (7) $^3\Sigma^+$ states around the internuclear distance of 3.9, 5.1, and 7.6 Å, respectively. These are important in identifying the corresponding Ω states discussed later in this section.

In general, the equilibrium bond distances obtained from PP1 are slightly overestimated, whereas those from PP2 tend to be underestimated compared with the experimental values listed in Table II. The overall agreement with experimental values is slightly better for PP2 than for PP1 in most cases, where the discrepancy does not exceed 0.05 Å apart from the (1) $^3\Delta$ state. The experimental value for this state, however, seems a bit too large in comparison with all theoretical values listed in the table, except for the one obtained with PP1 which suffers from overestimation by 0.1 Å. As for the bond distances obtained by Allouche *et al.*, the deviation from the experiments is a bit larger than it is for the PP2 results of this study in most cases. In particular, recently obtained experimental bond distances for the (2) $^1\Sigma^+$ and (5) $^1\Sigma^+$ states are better reproduced by the present work. Recent theoretical values of Zaitsevskii *et al.* obtained at the level of the many-body multipartitioning perturbation theory (MPPT) also agree better with the present equilibrium bond lengths in comparison with other theoretical values. For the transition energies (T_e), however, our values show much larger deviations from the experiments compared with the theoretical values of Allouche *et al.* This is perhaps not surprising since the angular moment dependent CPPs used in the latter were fitted to reproduce the atomic transition energies. These l-dependent one-electron CPPs are capable of producing extremely accurate values of transition energies, as shown in Table II, which seem to be the best choice in this case. This can also be easily seen from a comparison with the transition energies obtained by Pavolini *et al.*,[8] which incorporated core-valence contributions in a second-order perturbation scheme.[23] The improvement made on the transition energies by the use of different CPP schemes was noted by the authors of Ref. 9 before. The states showing the largest deviation from the values in Ref. 9 are the ones involving the atomic d states. This is expected from the discrepancy in the atomic asymptotes noted earlier. If we take the experimental transition energy at an infinite nuclear distance (T_∞) and adjust the calculated T_e accordingly, we obtain a much better agreement for these states. For example, the discrepancy between the present and the values of Ref. 9 for the (4) $^1\Sigma^+$ and (3) $^1\Pi$ states dissociating to $Rb(5s)+Cs(5d)$ is reduced by an order of magnitude by this adjustment [e.g., from 755 to 75 cm^{-1} for the (4) $^1\Sigma^+$ state]. Care must be taken, however, as this adjustment does not guarantee a systematic improvement for all states especially in cases of strong coupling between neighboring states. The (1) $^3\Sigma^+$ state shows the largest deviation in the spectroscopic constants reported here. This may be attributed to the highly repulsive nature of this state, which makes it difficult to predict the properties around the minimum of the potential energy profile.

The permanent dipole moments as a function of the internuclear distance are useful in the study of the changing nature of the electronic wave function proceeding on adiabatic surfaces. The experimental determination of such values is difficult to obtain, and the sign of the dipole moment cannot be determined. We therefore report the R-dependent permanent dipole moment of RbCs in Figs. 1–4. The abrupt change in the dipole moment distribution between the (5) and (6) $^1\Sigma^+$ states at 8.3 Å (Fig. 1) is consistent with the avoided crossing between these two states. Three avoided crossings among $^3\Sigma^+$ states mentioned earlier are also well indicated by the crossing of R-dependent dipole moments occurring between (2) and (3) at 4 Å, between (5) and (6) at 5.1 Å, and between (6) and (7) $^3\Sigma^+$ states at 7.6 Å, identical to the regions of internuclear distances exhibiting avoided crossings. The positive sign of the permanent dipole moment indicates Rb^+Cs^-. We note that there are only few R-dependent dipole moment functions available in the literature for this molecule. In fact, there is only one other set of such data from Zaitsevskii *et al.* They reported the dipole moment functions for the $^1\Pi$ states over a large range of internuclear distances, which closely resemble the results of this study. More recently, Aymar and Dulieu carried out a careful analysis of basis set effects and the core-core correlation contribution to the variation of the dipole moments for mixed heteronuclear alkali dimers and reported their results for the $X\ ^1\Sigma^+$ and $a\ ^3\Sigma^+$ states.[12] There are very recent all-electron results for these states by Kotochigova and Tiesinga.[13] For the purpose of comparison we list the available permanent dipole moment of the ground state RbCs in Table III. There is, in general, a good agreement between theoretical values for the ground state permanent dipole moment, whereas the empirical value obtained from dipole po-

TABLE II. Selected spectroscopic constants of RbCs. The second column shows an atomic dissociation limit for each state. For potential energy curves see Ref. 22.

$^1\Sigma^+$			R_e (Å)	ω_e (cm^{-1})	B_e (10^{-2} cm^{-1})	T_e (cm^{-1})	D_e (cm^{-1})
(1)	$5s+6s$	This work (PP2)[a]	4.364	49.09	1.689	0	4033
		This work (PP1)[b]	4.474	52	···	0	···
		Theor.[c]	4.379	51.35	1.690	0	3873
		Theor.[d]	4.385	45.60	···	0	4183
		Expt.[e]	4.418	50.01	1.660	0	3842
(2)	$5s+6p$	This work (PP2)[a]	5.137	36.11	1.219	10 356	5162
		This work (PP1)[b]	5.177	37	···	10 026	5225
		Theor.[c]	5.069	37.73	1.261	10 065	···
		Theor.[d]	4.991	39.71	···	10 343	5735
		Theor.[f]	5.16	37.2	···	10 132	···
		Expt.[g]	5.175	36.65	···	10 037.83	···
(3)	$5p+6s$	This work (PP2)[a]	5.527	26.67	1.053	13 402	3329
		This work (PP1)[b]	5.519	29	···	12 965	3377
		Theor.[c]	5.434	28.75	1.098	13 060	···
		Theor.[d]	5.364	32.96	···	13 397	3738
		Theor.[f]	5.54	29.3	···	13 061	···
		Expt.[e]	5.526	28.48	1.061	13 052.694	3527
(4)	$5s+5d$	This work (PP2)[a]	5.639	21.80	1.012	17 429	1826
		This work (PP1)[b]	5.600	23	···	16 568	1691
		Theor.[c]	5.543	23.12	1.055	16 674	···
		Theor.[d]	5.272	36.98	···	15 934	2421
		Theor.[f]	5.520	24.0	···	16 747	···
		Expt.[h]	···	24.51	···	16 626.6	···
(5)	$5s+7s$	This work (PP2)[a]	4.933	41.97	1.322	18 701	3805
		This work (PP1)[b]	4.967	40	···	18 481	3812
		Theor.[c]	4.871	41.37	1.366	18 562	···
		Theor.[d]	4.754	48.33	···	18 902	3946
		Theor.[f]	4.95	40.1	···	18 551	···
		Expt[i]	4.951	39.2	···	18 564.6	···
(6)	$4d+6s$	This work (PP2)[a]	5.448	31.78	1.084	19 897	3642
		This work (PP1)[b]	5.436	36.00	···	19 477	3550
		Theor.[c]	5.332	35.35	1.140	19 624	···
		Theor.[d]	5.282	37.50	···	19 657	3887
		Theor.[f]	5.408	35.2	···	19 522	···
(7)	$6s+6s$	This work (PP2)[a]	5.124	34.32	1.225	21 475	2615
		This work (PP1)[b]	5.167	35	···	21 151	2646
		Theor.[c]	5.074	35.30	1.259	21 273	···
		Theor.[d]	5.076	38.46	···	21 553	2788
		Theor.[f]	5.17	35.3	···	21 252	···
		Expt.[e]	5.118	35.04	1.237	21 230.884	2745
$^3\Sigma^+$							
(1)	$5s+6s$	This work (PP2)[a]	6.566	···	···	3 917	116
		This work (PP1)[b]	6.295	12	···	3 417	245
		Theor.[c]	5.843	42.84	0.949	3 633	···
		Theor.[d]	5.626	30.67	···	2 600	1587
(2)	$5s+6p$	This work (PP2)[a]	5.522	30.87	1.055	12 925	2593
		This work (PP1)[b]	5.461	31	···	12 582	2668
		Theor.[c]	5.309	32.20	1.150	12 635	···
		Theor.[d]	5.464	28.52	···	13 114	2964
(3)	$5p+6s$	This work (PP2)[a]	4.709	39.62	1.451	16 084	647
		This work (PP1)[b]	4.714	39	···	15 527	816
		Theor.[c]	4.609	38.98	1.526	15 526	···
		Theor.[d]	4.431	64.57	···	14 792	2343

TABLE II. (*Continued.*)

$^3\Sigma^+$			R_e (Å)	ω_e (cm^{-1})	B_e (10^{-2} cm^{-1})	T_e (cm^{-1})	D_e (cm^{-1})
(4)	$5s+5d$	This work (PP2)[a]	6.926	26.71	0.671	18 569	686
		This work (PP1)[b]	7.127	23	⋯	17 763	496
		Theor.[d]	6.963	30.82	⋯	18 022	333
(5)	$5s+7s$	This work (PP2)[a]	6.120	53.70	0.859	19 782	2723
		This work (PP1)[b]	5.912	57	⋯	19 623	3031
		Theor.[d]	5.755	68.30	⋯	19 585	3263
(6)	$4d+6s$	This work (PP2)[a]	5.407	48.61	1.101	21 042	2497
		This work (PP1)[b]	5.149	73	⋯	20 613	2415
		Theor.[d]	5.354	51.34	⋯	21 051	2493
(7)	$6s+6s$	This work[a]	5.522	41.03	1.055	21 907	2184
		Theor.[d]	5.212	62.89	⋯	21 830	2512
$^1\Pi$							
(1)	$5s+6p$	This work (PP2)[a]	4.657	37.93	1.483	13 873	1645
		This work (PP1)[b]	4.79	37	⋯	13 750	1500
		Theor.[c]	4.676	38.62	1.482	13 753	⋯
		Theor.[d]	4.747	33.16	⋯	14 152	1926
		Theor.[f]	4.72	35.4	⋯	13 814	⋯
(2)	$5p+6s$	This work (PP2)[a]	5.208	30.72	1.186	15 287	1444
		This work (PP1)[b]	5.230	34	⋯	14 879	1464
		Theor.[c]	5.119	33.36	1.237	15 046	⋯
		Theor.[d]	4.941	40.33	⋯	15 003	2132
		Theor.[f]	5.20	33.1	⋯	14 987	⋯
		Expt[e]	5.164	32.93	1.215	14 963.622	1616
(3)	$5s+5d$	This work (PP2)[a]	4.920	20.63	1.329	18 378	877
		This work (PP1)[b]	5.237	21	⋯	17 542	716
		Theor.[c]	5.060	20.42	1.266	17 633	⋯
		Theor.[d]	5.041	27.80	⋯	17 065	1290
		Theor.[f]	5.07	22.8	⋯	17 598	⋯
		Expt.[h]	⋯	22.53	⋯	17 418.9	⋯
(4)	$4d+6s$	This work (PP2)[a]	5.092	29.56	1.241	21 294	2245
		This work (PP1)[b]	5.16	30	⋯	20 923	2104
		Theor.[c]	5.074	30.70	1.272	21 034	⋯
		Theor.[d]	5.066	36.95	⋯	20 977	2567
		Theor.[f]	5.16	31	⋯	20 959	⋯
		Expt.[e]	5.117	30.24	1.238	20 896.952	2745
(5)	$5s+7p$	This work (PP2)[a]	5.081	34.79	1.246	21 926	3903
		This work (PP1)[b]	5.119	35	⋯	21 638	3947
		Theor.[c]	5.016	35.79	1.288	21 793	⋯
		Theor.[d]	4.930	39.37	⋯	22 243	4146
		Expt.[e]	5.071	35.67	⋯	21 744.774	3981
$^3\Pi$							
(1)	$5s+6p$	This work (PP2)[a]	4.294	48.38	1.745	8 980	6538
		This work (PP1)[b]	4.396	53	⋯	8 939	6311
		Theor.[c]	4.287	53.05	1.763	8 838	⋯
		Theor.[d]	4.230	46.53	⋯	9 804	6274
(2)	$5p+6s$	This work (PP2)[a]	5.007	29.29	1.283	15 877	854
		This work (PP1)[b]	5.069	30	⋯	15 342	1001
		Theor.[c]	4.953	32.13	1.321	15 398	⋯
		Theor.[d]	4.886	31.48	⋯	15 008	2127
(3)	$5s+5d$	This work (PP2)[a]	4.879	30.19	1.351	18 249	1006
		This work (PP1)[b]	5.222	15	⋯	17 696	562
		Theor.[c]	4.977	23.84	1.308	17 835	⋯
		Theor.[d]	5.259	21.79	⋯	17 551	804

TABLE II. (*Continued.*)

$^3\Pi$			R_e (Å)	ω_e (cm^{-1})	B_e (10^{-2} cm^{-1})	T_e (cm^{-1})	D_e (cm^{-1})
(4)	$4d+6s$	This work (PP2)[a]	5.483	32.05	1.070	19 869	3670
		This work (PP1)[b]	5.420	34	⋯	19 384	3643
		Theor.[c]	5.350	33.30	1.132	19 517	⋯
		Theor.[d]	5.164	37.83	⋯	19 369	4176
(5)	$5s+7p$	This work (PP2)[a]	5.041	35.76	1.266	21 665	4165
		This work (PP1)[b]	5.079	37	⋯	21 386	4200
		Theor.[c]	4.865	42.14	⋯	22 046	⋯
		Theor.[d]	4.865	42.14	⋯	22 046	4343
$^1\Delta$							
(1)	$5s+5d$	This work (PP2)[a]	4.389	37.61	1.670	16 573	2682
		This work (PP1)[b]	4.571	37	⋯	16 185	2074
		Theor.[c]	4.443	40.18	1.642	16 143	⋯
		Theor.[d]	4.514	37.86	⋯	16 367	1978
(2)	$4d+6s$	This work (PP2)[a]	5.203	30.64	1.189	21 084	2455
		This work (PP1)[b]	5.275	40	⋯	20 507	2520
		Theor.[c]	5.146	32.92	1.224	20 657	⋯
		Theor.[d]	5.002	37.47	⋯	20 799	2745
$^3\Delta$							
(1)	$5s+5d$	This work (PP2)[a]	4.479	35.04	1.604	17 159	2096
		This work (PP1)[b]	4.690	37	⋯	16 675	1583
		Theor.[c]	4.556	36.45	1.561	16 702	⋯
		Theor.[d]	4.516	36.79	⋯	16 511	1844
		Expt.[j]	4.59	36.51	⋯	16 481.65	1863
(2)	$4d+6s$	This work (PP2)[a]	5.169	32.49	1.204	21 297	2243
		This work (PP1)[b]	5.226	38	⋯	20 812	2215
		Theor.[c]	5.102	34.61	1.245	20 917	⋯
		Theor.[d]	5.056	36.98	⋯	31 329	2215

[a]Stuttgart pseudopotential of Lim *et al.* from Ref. 16.
[b]Stuttgart pseudopotential of Leininger from Ref. 15.
[c]Ref. 9.
[d]Ref. 8.
[e]Ref. 26.
[f]Ref. 11.
[g]Ref. 6.
[h]Ref. 27.
[i]Ref. 28.
[j]Ref. 29.

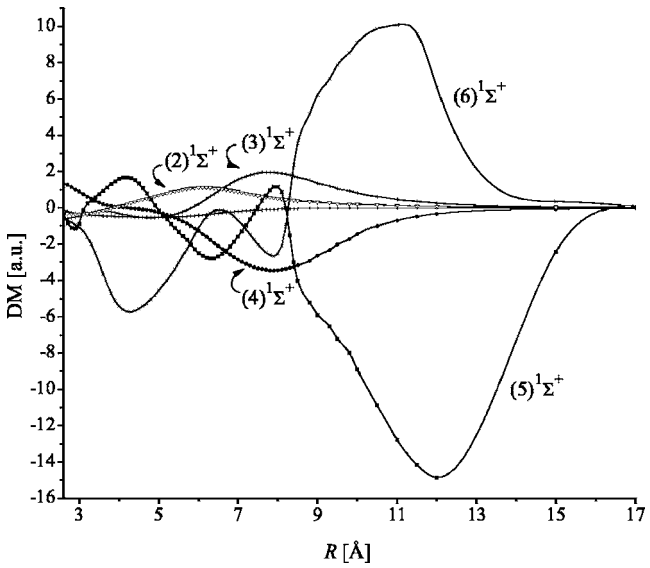

FIG. 1. Permanent dipole moments for the $^1\Sigma^+$ states of RbCs as a function of the internuclear distance. See Ref. 22 for the numerical data.

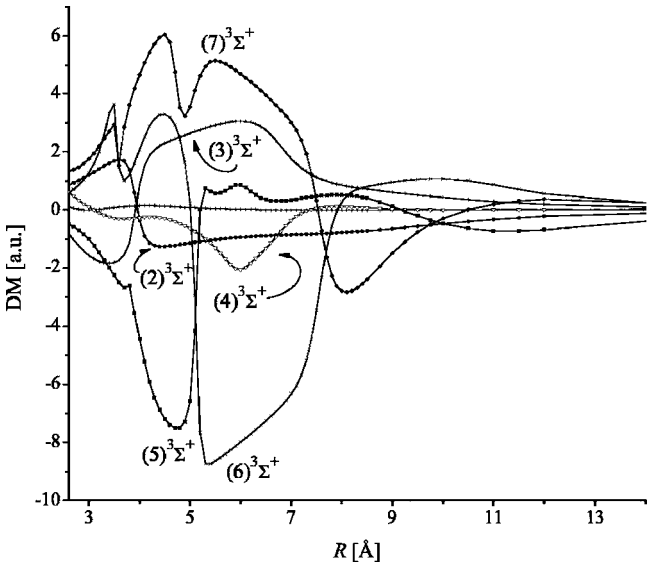

FIG. 2. Permanent dipole moments for the $^3\Sigma^+$ states of RbCs as a function of the internuclear distance. See Ref. 22 for the numerical data.

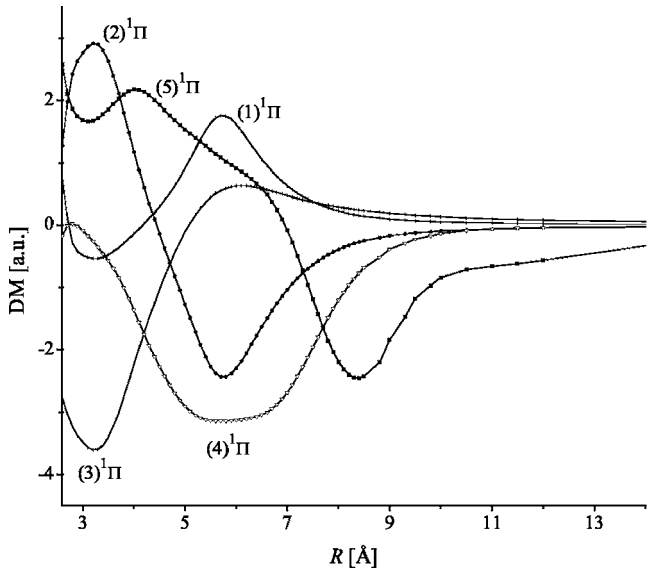

FIG. 3. Permanent dipole moments for the $^1\Pi$ states of RbCs as a function of the internuclear distance. See Ref. 22 for the numerical data.

larizabilities is almost twice as large. Kotochigova and Tiesinga's value of 0.06 D (Ref. 13) for the $a\ ^3\Sigma^+$ state at the equilibrium separation is in good agreement with our value of 0.059 D if we take the equilibrium separation of Ref. 9, i.e., R_e=5.843 Å. At the minimum bond separation of this study, however, which is somewhat larger (R_e=6.566 Å), the calculated dipole moment is much smaller. It is still interesting to compare the equilibrium bond distance between the $a\ ^3\Sigma^+$ and (1) 0^- states which results purely from the former. Our calculated bond distance between these two states shows a smaller deviation from each other than the values from Refs. 9 and 10, which may suggest that the bond distance for the $a\ ^3\Sigma^+$ state may be slightly underestimated in other calculations. Moreover, the two sets of pseudopotentials tested in this study give values closer to each other than to other theoretical values. The bond distance at which the dipole

TABLE III. Permanent dipole moment of RbCs in the $X\ ^1\Sigma^+$ state at the equilibrium bond distance (R=R_e). All values are in debye (1 a.u. =2.541 5805 9 D).

Method	Ref.	Dipole moment
ECP+CI	This work	−1.29
RCI-VB[a]	13	−1.25
ECP+CI	30	−1.26
ECP+CI	12	−1.205
Empirical	31	2.39

[a]All-electron relativistic configuration interaction valence-bond method.

moment of the $a\ ^3\Sigma^+$ state was determined in Kotochigova's study seems to be R=6.09 Å, judging by the table of dipole moments given in their paper, at which we obtain a dipole moment (DM)=0.027 D. In Fig. 5 we plotted the permanent dipole moment functions obtained in the present study against those obtained by Kotochigova[13] for comparison. Since the results of Ref. 13 already contain spin-orbit effects, we plot Ω states but still follow the notations as used in Ref. 13 for their results in the figure. The dipole moments of this work tend to be smaller in magnitude for the $a\ ^3\Sigma^+$ state although the overall shape is similar. For the $X\ ^1\Sigma^+$ state there is a more notable discrepancy where the present work estimates larger moments in magnitude than the all-electron values over the intermediate values of nuclear separation. A simple interpolation of the dipole moment plot of Aymar and Dulien[12] suggests that their values may lie closer to the present ones over this range of R.

Spin-orbit effects were accounted for by the use of two-component pseudopotentials of Lim *et al.* Selected spectroscopic constants extracted from the PECs are shown in Tables IV–VII for $\Omega=0^+$, 0^-, 1, 2, and 3 states, respectively. Via the Dunham-type analysis we also derived and listed the spectroscopic constants obtained from the tables of energies available through all-electron calculations of Kotochigova for comparison.[24] In general, potential energy curves exhibit

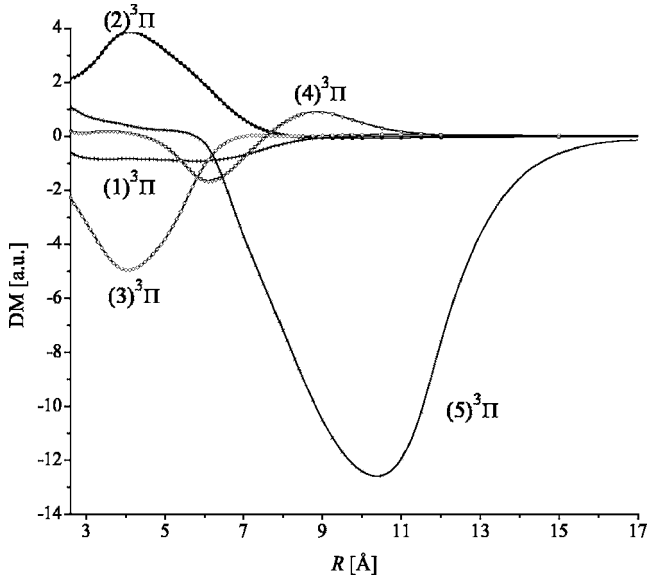

FIG. 4. Permanent dipole moments for the $^3\Pi$ states of RbCs as a function of the internuclear distance. See Ref. 22 for the numerical data.

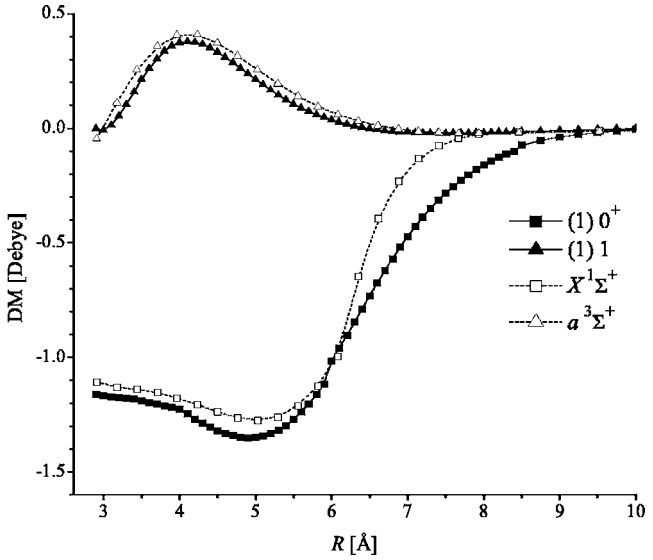

FIG. 5. Permanent dipole moment (DM) function of RbCs. The positive sign indicate Rb^+Cs^-. The solid line is used for the present work and the dashed line for Ref. 13.

TABLE IV. Selected spectroscopic constants for the $\Omega=0^+$ states of RbCs. For potential energy curves see Ref. 22.

0^+	$\Lambda\Sigma$		R_e (Å)	ω_e (cm^{-1})	B_e (10^{12} cm^{-1})	T_e (cm^{-1})
(1)	$(1)^1\Sigma^+$	This work	4.364	49.13	1.69	0
		Theor.[a]	4.380	51.3	1.69	0
(2)	$(1)^3\Pi-(2)^1\Sigma^+$	This work	4.294	48.43	1.74	8 976
		Theor.[a]	4.308	52.0	1.75	8 630
		Theor.[b]	4.250	53.49	1.78	
(3)	$(2)^1\Sigma^+-(1)^3\Pi$	This work	5.112	40.08	1.23	10 870
		Theor.[a]	4.974	45.9	···	10 160
		Theor.[b]	5.026	55.96	1.27	
(4)	$(3)^1\Sigma^+$	This work	5.526	26.68	1.05	13 400
		Theor.[a]	5.434	28.9	1.10	13 053
(5)	$(2)^3\Pi$	This work	5.008	29.17	1.28	15 880
		Theor.[a]	4.942	29.8	1.33	15 359
(6)	$(3)^3\Pi-(4)^1\Sigma^+$	This work	5.637	21.86	1.01	17 430
		Theor.[a]	5.543	23.4	1.05	16 673
(7)	$(4)^1\Sigma^+-(3)^3\Pi$	This work	4.880	30.20	1.35	18 251
		Theor.[a]	5.027	···	···	17 802
(8)	$(5)^1\Sigma^+$	This work	4.933	41.95	1.32	18 701
		Theor.[a]	4.870	41.4	1.37	18 564
(9)	$(4)^3\Pi-(6)^1\Sigma^+$	This work	5.469	31.60	1.08	19 854
		Theor.[a]	5.343	35.0	1.40	19 323
(10)	$(6)^1\Sigma^+-(4)^3\Pi$	This work	5.463	31.76	1.08	19 913
		Theor.[a]	5.346	34.6	1.13	19 672
(11)	$(7)^1\Sigma^+$	This work	5.203	30.61	1.19	21 085
		Theor.[a]	5.067	35.0	1.26	21 244

[a]Reference 10.
[b]Obtained via the Dunham-type analysis from all-electron relativistic configuration interaction valence model (RCI-VB) calculations of Ref. 13.

TABLE V. Selected spectroscopic constants for the $\Omega=0^-$ states of RbCs. For potential energy curves see Ref. 22.

0^-	$\Lambda\Sigma$		R_e (Å)	ω_e (cm^{-1})	B_e (10^{-2} cm^{-1})	T_e (cm^{-1})
(1)	$(1)^3\Sigma^+$	This work	6.467	9.52	0.77	3 917
		Theor.[a]	6.179	12.6	0.85	3 607
(2)	$(1)^3\Pi-(2)^3\Sigma^+$	This work	4.294	48.40	1.74	8 981
		Theor.[a]	4.300	52.7	1.75	8 675
		Theor.[b]	4.203	50.54	1.82	
(3)	$(2)^3\Sigma^+-(1)^3\Pi$	This work	5.421	30.93	1.09	12 922
		Theor.[a]	5.310	32.2	1.15	12 636
		Theor.[b]	5.613	29.65	1.02	
(4)	$(2)^3\Pi$	This work	5.002	29.23	1.29	15 876
		Theor.[a]	4.877	30.8	1.36	15 215
(5)	$(3)^3\Sigma^+$	This work	4.639	43.46	1.50	16 099
		Theor.[a]	4.685	39.8	1.48	15 627
(6)	$(3)^3\Pi$	This work	4.879	30.11	1.35	18 250
		Theor.[a]	4.970	···	···	17 788
(7)	$(4)^3\Sigma^+$	This work	5.201	32.18	1.19	18 726
		Theor.[a]	5.118	34.5	1.24	18 467
(8)	$(4)^3\Pi-(5)^3\Sigma^+$	This work	6.017	53.71	0.89	19 779
		Theor.[a]	5.300	···	···	19 408
(9)	$(5)^3\Sigma^+-(4)^3\Pi$	This work	5.801	73.73	0.96	19 972
		Theor.[a]	5.713	57.9	0.99	19 535
(10)	$(6)^3\Sigma^+$	This work	5.255	57.47	1.17	21 035
		Theor.[a]	5.174	47.9	1.21	20 712
(11)	$(5)^3\Pi-(7)^3\Sigma^+$	This work	5.046	35.75	1.26	21 671
		Theor.[a]	5.012	34.8	1.29	21 471

[a]Refrence 10.
[b]Obtained via the Dunham-type analysis from RCI-VB calculations of Ref. 13.

TABLE VI. Selected spectroscopic constants for the $\Omega=1$ states of RbCs. For potential energy curves see Ref. 22.

1	$\Lambda\Sigma$		R_e (Å)	ω_e (cm^{-1})	B_e (10^{-2} cm^{-1})	T_e (cm^{-1})
(1)	$(1)^3\Sigma^+$	This work	6.468	9.71	0.77	3 917
		Theor.[a]	6.178	13.0	0.85	3 608
(2)	$(1)^3\Pi-(2)^3\Sigma^+$	This work	4.293	48.38	1.75	8 980
		Theor.[a]	4.291	52.8	1.76	8 833
		Theor.[b]	4.265	50.44	1.77	
(3)	$(1)^1\Pi-(2)^3\Sigma^+-(1)^3\Pi$	This work	5.421	30.79	1.09	12 915
		Theor.[a]	5.325	29.1	1.14	12 635
		Theor.[b]	5.619	28.60	1.02	
(4)	$(2)^3\Sigma^+-(1)^1\Pi$	This work	4.674	43.62	1.48	13 869
		Theor.[a]	4.616	40.8	1.52	13 743
		Theor.[b]	4.910	49.31	1.33	
(5)	$(2)^1\Pi$	This work	5.209	30.66	1.19	15 290
		Theor.[a]	5.122	35.2	1.24	15 039
(6)	$(2)^3\Pi$	This work	5.007	29.22	1.28	15 877
		Theor.[a]	4.894	31.1	1.35	15 375
(7)	$(3)^3\Sigma^+$	This work	4.642	43.95	1.49	16 099
		Theor.[a]	4.696	41.8	1.47	15 611
(8)	$(1)^3\Delta$	This work	4.478	35.25	1.60	17 159
		Theor.[a]	4.559	36.3	1.56	16 664
		Expt.[c]	4.59	36.51	⋯	16 481.7
(9)	$(3)^3\Pi$	This work	4.879	30.18	1.35	18 250
		Theor.[a]	5.061	20.3	1.27	17 634
(10)	$(3)^1\Pi$	This work	4.919	20.80	1.33	18 378
		Theor.[a]	4.976	23.6	1.31	17 841
(11)	$(4)^3\Sigma^+$	This work	5.202	31.97	1.19	18 726
		Theor.[a]	5.115	33.7	1.24	18 467
(12)	$(5)^3\Sigma^+$	This work	5.425	43.46	1.09	19 864
		Theor.[a]	5.345	⋯	⋯	19 518
(13)	$(4)^3\Pi$	This work	5.809	73.85	0.95	19 972
		Theor.[a]	5.669	58.0	1.01	19 612
(14)	$(6)^3\Sigma^+$	This work	5.261	58.12	1.16	21 034
		Theor.[a]	5.205	42.6	1.20	20 728
(15)	$(2)^3\Delta$	This work	5.152	37.41	1.21	21 270
		Theor.[a]	5.122	35.0	1.24	20 913
(16)	$(4)^1\Pi$	This work	5.132	31.87	1.23	21 298
		Theor.[a]	5.058	39.1	1.27	21 029
(17)	$(7)^3\Sigma^+$	This work	5.422	40.95	1.09	21 908
		Theor.[a]	4.997	33.3	1.30	21 519

[a]Reference 10.
[b]Obtained via the Dunham-type analysis from RCI-VB calculations of Ref. 13.
[c]Reference 29.

similar shapes for all Ω states to those obtained by Fahs *et al.* The parent $\Lambda\Sigma$ states giving rise to each Ω state and the corresponding dissociation limit are identified by the superposition of nearby states. The decomposition of Ω states in terms of $\Lambda\Sigma$ notations is given in the tables where multiple entries of $\Lambda\Sigma$ terms for a given Ω state show the change in the wave function for that Ω state over a range of the internuclear separation. Most potential energy curves show complicated forms with avoided crossings resulting from the crossing of parent $\Lambda\Sigma$ states. There are exceptions, however, which include, for $\Omega=0^+$, the lowest (1) 0^+, (4) 0^+, and (5) 0^+ states, for which the parent $\Lambda\Sigma$ states are identified as (1) $^1\Sigma^+$, (3) $^1\Sigma^+$, and (2) $^3\Pi$ states, respectively. We note a sharp avoided crossing around 5.4 Å between the (2) 0^+ and (3) 0^+ states whose parent states, in the vicinity of the minimum, are the bound (1) $^3\Pi$ and (2) $^1\Sigma^+$ states, respectively. The effects of the sharp avoided crossing is also evident in the variation of the permanent dipole moment as a function of the internuclear distance as indicated by the abrupt change at around 5.4 Å (Fig. 6). In order to clearly demonstrate the effects of the spin-orbit coupling on the *R*-dependent permanent dipole moment function, the $\Lambda\Sigma$ moment functions are also plotted in the figure. The sudden undulation around 5.4 Å is indicative of the change in the wave function describing the particular state due to the spin-orbit interaction. Spin-orbit effects on the dipole moment are significant only at the regions of the avoided crossing between the parent $\Lambda\Sigma$ states. At other internuclear separations the spin-orbit coupling is rather small. The large relativistic effects affecting the magnitude of dipole moments noted for KRb in the work of Kotochigova *et al.*, therefore, seems likely to be the effects of scalar relativity rather than spin-orbit effects.[25] Turn-

TABLE VII. Selected spectroscopic constants for the $\Omega=2$ and 3 states of RbCs. For potential energy curves see Ref. 22.

2	$\Lambda\Sigma$		R_e (Å)	ω_e (cm^{-1})	B_e (10^{-2} cm^{-1})	T_e (cm^{-1})
(1)	$(1)^3\Pi$	This work	4.293	48.40	1.745	8 980
		Theor.[a]	4.278	53.1	1.770	9 007
(2)	$(1)^1\Delta-(2)^3\Pi$	This work	5.007	29.29	1.283	15 877
		Theor.[a]	4.948	31.5	1.320	15 478
(3)	$(2)^3\Pi-(1)^1\Delta-(3)^3\Pi$	This work	4.392	33.67	1.664	16 575
		Theor.[a]	4.428	44.8	1.650	16 134
(4)	$(1)^3\Delta$	This work	4.478	35.21	1.604	17 159
		Theor.[a]	4.557	36.4	1.560	16 708
(5)	$(3)^3\Pi-(1)^3\Delta$	This work	4.879	30.19	1.352	18 250
		Theor.[a]	4.970	···	···	17 884
(6)	$(4)^3\Pi$	This work	5.203	30.64	1.189	21 085
		Theor.[a]	5.371	32.2	1.120	19 655
(7)	$(2)^1\Delta$	This work	5.173	27.30	1.204	21 088
		Theor.[a]	5.146	33.0	1.220	2 066
(8)	$(2)^3\Delta$	This work	5.169	32.48	1.204	21 297
		Theor.[a]	5.102	34.6	1.240	20 920
3						
(1)	$(1)^3\Delta$	This work	4.478	35.20	1.605	17 042
		Theor.[a]	4.556	36.5	1.560	16 745
(2)	$(2)^3\Delta$	This work	5.169	32.49	1.283	21 181
		Theor.[a]	5.099	35.2	1.204	20 930

[a]Reference 10.

ing back to the PECs, we note avoided crossings between (6) and (7) 0^+ caused by a mixing of the (4) $^1\Sigma^+$ and (3) $^3\Pi$ states. This occurs below 4 Å, i.e., below the equilibrium distance for either states, implying that at shorter nuclear distances, the (6) 0^+ and (7) 0^+ states correlate to the (3) $^3\Pi$ and (4) $^1\Sigma^+$ states, respectively. Around the minima, however, these Ω states mutually switch their respective character and correlate to the (4) $^1\Sigma^+$ and (3) $^3\Pi$ states. This is reflected in their equilibrium spectroscopic constants. An opposite case to this is an avoided crossing between the (9) 0^+ and (10) 0^+ states, which occurs at a nuclear distance longer than the equilibrium bond distances of the corresponding parent states. Therefore, at the minimum, the (9) 0^+ and (10) 0^+ states are characterized by the respective (4) $^3\Pi$ and (6) $^1\Sigma^+$ states, which then correlate adiabatically to the (6) $^1\Sigma^+$ and (4) $^3\Pi$ states at the dissociation, respectively. As the parent $\Lambda\Sigma$ states lie very close to each other around the minimum (within 0.04 Å and in less than 30 cm^{-1} in T_e), it is not easy to accurately characterize the corresponding Ω states in a quantitative manner. Qualitatively, however, the slightly longer equilibrium bond distance for (9) 0^+ than for (10) 0^+ is consistent with the trend predicted for the parent (4) $^3\Pi$ and (6) $^1\Sigma^+$ states at the minimum. The interaction between these states are, nevertheless, not simple to describe, which may well be the source of discrepancy between the present and previous spectroscopic constants listed in Table IV. In particular, the qualitative correlation between these two sets of Ω and $\Lambda\Sigma$ states was not visible in the work reported previously.

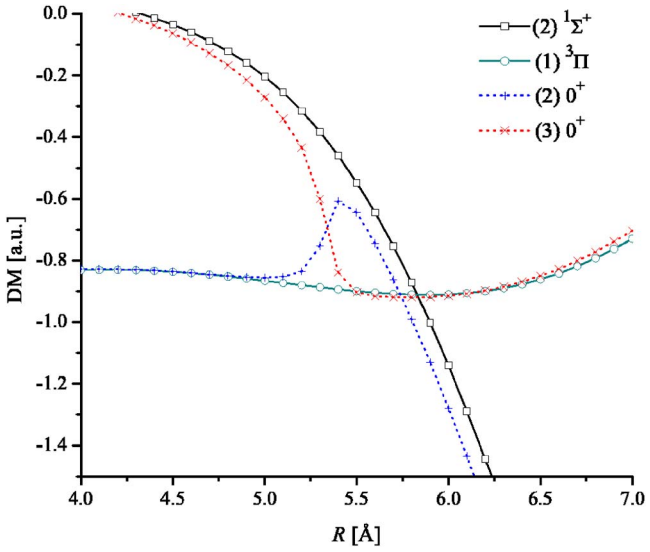

FIG. 6. (Color online) Permanent dipole moments for selected $\Omega=0^+$ states (dotted line) of RbCs as a function of the internuclear distance. Plotted also are the corresponding parent $\Lambda\Sigma$ states (solid line).

As for the $\Omega=0^-$ states, the main $\Lambda\Sigma$ states responsible are the $^3\Sigma^+$ and $^3\Pi$ states. The lowest (1) 0^- state derives purely from the (1) $^3\Sigma^+$ state, whereas the next two lowest states show an avoided crossing at around 7 Å. This is due to the spin-orbit coupling between the (1) $^3\Pi$ and (2) $^3\Sigma^+$ states and is clearly indicated by the change in the dipole moment function, as shown in Fig. 7. The next two states, mainly (4) and (5) 0^- correspond to the (2) $^3\Pi$ and (3) $^3\Sigma^+$ states, respectively, which are, to the best approximation, not affected by spin-orbit-induced avoided crossing although they approach each other very closely in the vicinity of their minima. The hump in the (5) 0^- around 6.6 Å is, therefore, characteristic of the parent (3) $^3\Sigma^+$ state rather than a result of the spin-orbit interaction. Furthermore, the avoided crossing around 3.9 Å for the (3) and (5) 0^- states already exists

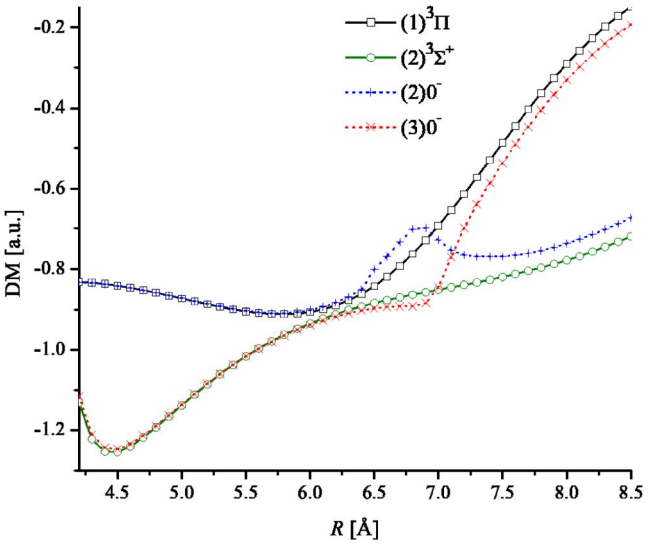

FIG. 7. (Color online) Permanent dipole moments for selected $\Omega=0^-$ states (dotted line) of RbCs as a function of the internuclear distance. Plotted also are the corresponding parent $\Lambda\Sigma$ states (solid line).

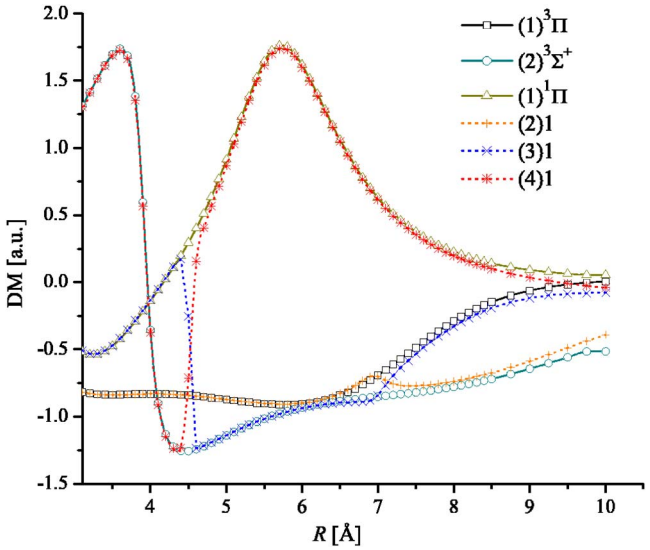

FIG. 8. (Color online) Permanent dipole moments for selected $\Omega=1$ states (dotted line) of RbCs as a function of the internuclear distance. Plotted also are the corresponding parent $\Lambda\Sigma$ states (solid line).

between the parent (2) and (3) $^3\Sigma^+$ states and hence not related to the spin-orbit interaction. The higher states, however, exhibit complicated structures due to the spin-orbit interaction. In particular, the potential energy curves for the four highest states, i.e., (8)–(11) 0^- are derived from $\Lambda\Sigma$ states already affected by the avoided crossing among themselves, which makes it even more difficult to identify parent states. By the superposition of the most likely $\Lambda\Sigma$ states we endeavored to identify the origin of these Ω states at the vicinity of the minimum: (5) $^3\Sigma^+$, (4) $^3\Pi$, (6) $^3\Sigma^+$, and (5) $^3\Pi$ for the (8)–(11) 0^-, respectively.

The $\Omega=1$ states occur from the interaction of four sets of $\Lambda\Sigma$ states, mainly those of $^3\Sigma^+$, $^1\Pi$, $^3\Pi$, and $^3\Delta$. The lowest states lie very close to the (1) $^3\Sigma^+$ state for the entire internuclear distances considered in this study. Noted for the next three Ω states is a mixing of three $\Lambda\Sigma$ parent states giving two avoided crossings at 4.5 and 7 Å. From the dipole moment functions shown in Fig. 8, one can easily see a spin-orbit-induced crossing between the (3) and (4) 1 states at 4.5 Å due to the coupling of (1) $^1\Pi$ and (2) $^3\Sigma^+$. The interaction of the (2) $^3\Sigma^+$ state with the (1) $^3\Pi$ state gives rise to a second crossing between the (2) and (3) 1 states around 7 Å, which is expected from the (2) and (3) 0^- states, as seen from Fig. 7. As was the case for other Ω states, the higher lying states display complicated forms of potential energy curves. We report the following main parent $\Lambda\Sigma$ states around the minimum of each Ω state: (2) $^1\Pi$, (2) $^3\Pi$, (3) $^3\Sigma^+$, (1) $^3\Delta$, (3) $^3\Pi$, (3) $^1\Pi$, (4) $^3\Sigma^+$, (5) $^3\Sigma^+$, (4) $^3\Pi$, (6) $^3\Sigma^+$, (2) $^3\Delta$, (4) $^1\Pi$, and (7) $^3\Sigma^+$ for the (5)–(17) 1 states, respectively.

The last set of Ω states considered in this work, $\Omega=2$, results from the spin-orbit interaction among $^3\Pi$, $^1\Delta$, and $^3\Delta$ states. As was the case for all other Ω states, the lowest (1) 2 state can be traced back to a unique $\Lambda\Sigma$ parent state, mainly (1) $^3\Pi$. The three highest states, i.e., $\Omega=(6)$, (7), and (8) 2, also follow closely their respective parent (4) $^3\Pi$, (2) $^1\Delta$, and (2) $^3\Delta$ states in the entire range of internuclear distances considered here. The remaining four Ω states display avoided crossings, and at their minima the parent $\Lambda\Sigma$ states are identified as (2) $^3\Pi$, (1) $^1\Delta$, (1) $^3\Delta$, and (3) $^3\Pi$ for the (2), (3), (4), and (5) 2 states, respectively.

There is a reasonable overall agreement between the two sets of spectroscopic constants obtained by pseudopotential methods listed in Tables IV–VII for the Ω states, except for a couple of cases where the equilibrium bond length deviates from each other by more than 0.1 Å. There is, however, a

TABLE VIII. The location (R_{ac} in a_0) and the width (δ_{ac} in cm^{-1}) of selected avoided crossings as predicted from the potential energy curves of this study. For comparison other values reported in the literature are listed as well. The width is the minimum energy separation between two avoiding potential energy curves.

		States							
		(2)–(3) 0^+		(2)–(3) 0^-		(2)–(3) 1		(3)–(4) 1	
Method	Ref.	R_{ac}	Δ_{ac}	R_{ac}	δ_{ac}	R_{ac}	δ_{ac}	R_{ac}	δ_{ac}
SOPP-MRCI[a]	This work	10.2	182	13.2	136	13.2	136	8.5	142
SOPP-MRCI[b]	10	10.1	534	13.7	208	13.1	148	8.2	43
RCI-VB[c]	13	10	297	13.5	273	13.5	205	8.2	240

[a]Nonempirical spin-orbit pseudopotentials at the MRCI level.
[b]Semi-empirical spin-orbit pseudopotentials at the MRCI level.
[c]All-electron relativistic configuration interaction valence bond model.

larger deviation in the all-electron results of Kotochigova especially in the equilibrium bond distance compared with the two pseudopotential results. This should be taken for comparison purposes only as the authors did not give spectroscopic constants themselves but only the potential energies. In terms of the experimental bond distance for the (8) 1 state the theoretical values reported in Table VI seem to be underestimated, which is more severe for the present case with a discrepancy of about 0.1 Å. This trend is also evident in the vibrational frequencies for this state. As was the case for the $\Lambda\Sigma$ states, the transition energies of Ref. 10 obtained with *l*-dependent CPPs are expected to be superior to the present values. It is still interesting to compare the width and the location of some of the spin-orbit-induced avoided crossings reported in the literature (Table VIII). As can be seen, the width of the avoided crossing is underestimated by the present MRCI scheme compared with the all-electron valence-bond model of Kotochigova and Tiesinga. They noticed a significant difference in the width of the (2)–(3) 0^- and (3)–(4) 1 between their results and those of Fahs *et al.* Our results show that the width of these avoided crossings tends much more towards the all-electron calculations. Although the deviation from the all-electron results seems more systematic in our case than in Fahs *et al.*, it is difficult to judge from this comparison alone which set of pseudopotentials offers a better approximation in comparison with the all-electron case.

IV. CONCLUSION

We presented in this paper, the potential energy curves and the spectroscopic constants of a large number of electronic states of RbCs as calculated from the spin-averaged and two-component spin-orbit small-core energy-consistent pseudopotentials. This is the first application of nonempirical pseudopotentials to the spin-orbit states. Although the present transition energies may be improved by a better description of the core-valence correlation, provided here is a clear qualitative account for the effects of the spin-orbit coupling in terms of the potential energy curves as well as the *R*-dependent permanent dipole moments.

ACKNOWLEDGMENTS

This work was supported by a grant (M102kn010010-05K1401-01010) from the Center for Nanomechatronics & Manufacturing, one of the Frontier Research Programs supported by MOST, as well as the Korea Research Foundation (KRF-2004-041-C00161), the supercomputing center of KISTI, and CNRS. One of the authors (G.-H.J.) would like to thank the KOFST for the support through the 2005 Brain Pool program. The authors also like to express their gratitude to Professor Hermann Stoll of Stuttgart for helpful discussions.

[1] A. Fioretti, D. Comparat, A. Crubellier, O. Dulieu, F. Masnou-Seeuws, and P. Pillet, Phys. Rev. Lett. **80**, 4402 (1998).
[2] R. Wynar, R. Freeland, D. Han, C. Ryu, and D. Heinzen, Science **287**, 1016 (2000).
[3] F. Fatemi, K. Jones, P. Lett, and E. Tiesinga, Phys. Rev. A **66**, 053401 (2002).
[4] D. DeMille, Phys. Rev. Lett. **88**, 067901 (2002).
[5] M. G. Kozlov and D. DeMille, Phys. Rev. Lett. **89**, 133001 (2002).
[6] T. Bergeman, C. E. Fellows, R. F. Gutterres, and C. Amiot, Phys. Rev. A **67**, 050501(R) (2003).
[7] A. J. Kerman, J. M. Sage, S. Sainis, T. Bergeman, and D. DeMille, Phys. Rev. Lett. **92**, 153001 (2004).
[8] D. Pavolini, T. Gustavsson, F. Spiegelmann, and J.-P. Daudey, J. Phys. B **22**, 1721 (1989).
[9] A. R. Allouche, M. Korek, K. Fakherddin, A. Chaalan, M. Dagher, F. Taher, and M. Aubert-Frécon, J. Phys. B **33**, 2307 (2000).
[10] H. Fahs, A. R. Allouche, M. Korek, and M. Aubert-Frécon, J. Phys. B **35**, 1501 (2001).
[11] A. Zaitsevskii, E. A. Pazyuk, A. V. Stolyarov, O. Docenko, I. Klincare, O. Nikolayeva, M. Auzinsh, M. Tamanis, and R. Ferber, Phys. Rev. A **71**, 012510 (2005).
[12] M. Aymar and O. Dulieu, J. Chem. Phys. **122**, 204302 (2005).
[13] S. Kotochigova and E. Tiesinga, J. Chem. Phys. **123**, 174304 (2005).
[14] L. Morgus, P. Burns, R. D. Miles, A. D. Wilkins, U. Ogba, A. P. Hickman, and J. Huennekens, J. Chem. Phys. **122**, 144313 (2005).
[15] T. Leininger, A. Nicklass, W. Küchle, H. Stoll, M. Dolg, and A. Bergner, Chem. Phys. Lett. **255**, 274 (1996).
[16] I. S. Lim, P. Schwerdtfeger, B. Metz, and H. Stoll, J. Chem. Phys. **122**, 104103 (2005).
[17] W. Müller, J. Flesch, and W. Meyer, J. Chem. Phys. **80**, 3297 (1984).
[18] H. J. Werner, P. J. Knowles, R. D. Amos *et al.*, MOLPRO, Version 2002.1, a package of *ab initio* programs, Birmingham, UK, 2002.
[19] C. E. Moore, *Atomic Energy Levels*, Natl. Bur. Stand. (U.S.) Circ. No. 467 (U.S. GPO, Washington, D.C., 1952), Vol. II; reprinted as Natl. Stand. Ref. Data Ser. 35, 180 (1971); *Atomic Energy Levels*, Natl. Bur. Stand. (U.S.) Circ. No. 467, (U.S. GPO, Washington, D.C., 1958), Vol. III; reprinted as Natl. Stand. Ref. Data Ser. 35, 124 (1971).
[20] D. Edvardsson, S. Lunell, and C. M. Marian, Mol. Phys. **101**, 2381 (2003).
[21] C. E. Fellows, R. F. Gutterres, A. P. C. Campos, V. Vergès, and C. Amiot, J. Mol. Spectrosc. **197**, 19 (1999).
[22] See EPAPS Document No. E-JCPSA6-124-307621 for HTML files containing numerical data of this work. This document can be reached via a direct link in the online article's HTML reference section or via the EPAPS homepage (http://www.aip.org/pubservs/epaps.html).
[23] G. H. Jeung, J. P. Malrieu, and J. P. Daudey, J. Chem. Phys. **77**, 3571 (1982); G. H. Jeung, J. P. Daudey, and J. P. Malrieu, J. Phys. B **16**, 699 (1983).
[24] See EPAPS Document No. E-JCPSA6-123-305539.
[25] S. Kotochigova, P. S. Julienne, and E. Tiesinga, Phys. Rev. A **68**, 022501 (2003).
[26] T. Gustavsson, C. Amoit, and J. Cerges, Mol. Phys. **64**, 270 (1988); **64**, 293 (1988); Chem. Phys. Lett. **143**, 101 (1988).
[27] B. Kim and K. Yoshihara, J. Chem. Phys. **100**, 1849 (1994).
[28] Y. Yoon, Y. Lee, T. Kim, J. S. Ahn, Y. Jung, B. Kim, and S. Lee, J. Chem. Phys. **114**, 8926 (2001).
[29] B. Kim and K. Yoshihara, Chem. Phys. Lett. **212**, 271 (1993).
[30] G. Igel-Mann, U. Wedig, P. Fuentealba, and H. Stoll, J. Chem. Phys. **84**, 5007 (1986).
[31] V. Tarnovsky, M. Bunimovicz, L. Vuskovic, B. Stumpf, and B. Bederson, J. Chem. Phys. **98**, 3894 (1993).